Materials Science & Engineering A 615 (2014) 169–174

Contents lists available at ScienceDirect

Materials Science & Engineering A

journal homepage: www.elsevier.com/locate/msea

Short fatigue cracks nucleation and growth in lean duplex stainless steel LDX 2101

R. Strubbia [a,*], S. Hereñú [a], I. Alvarez-Armas [a], U. Krupp [b]

[a] Instituto de Física Rosario – CONICET, Universidad Nacional de Rosario, Argentina
[b] Faculty of Engineering and Computer Science, University of Applied Sciences Osnabrück, Germany

ARTICLE INFO

Article history:
Received 8 July 2014
Received in revised form
21 July 2014
Accepted 22 July 2014
Available online 30 July 2014

Keywords:
Duplex stainless steel
Fatigue
Crack nucleation and growth
Microstructure
EBSD

ABSTRACT

This work is focused on the fatigue damage of lean duplex stainless steels (LDSSs) LDX 2101. Special interest is placed on analyzing short fatigue crack behavior. In this sense, short crack initiation and growth during low cycle fatigue (LCF) and short crack nucleation during high cycle fatigue (HCF) of this LDSS have been studied. The active slip systems and their associated Schmid factors (SF) are determined using electron backscattered diffraction (EBSD). Additionally, the dislocation structure developed during cycling is observed by transmission electron microscopy (TEM). Regardless of the fatigue regime, LCF and HCF, short cracks nucleate along intrusion/extrusions in ferritic grains. Moreover, during the LCF phase boundaries decelerate short crack propagation. These results are rationalized by the hardness of the constitutive phases and the dependence of screw dislocation mobility in the ferrite phase on strain rate and stress amplitude.

1. Introduction

Duplex stainless steels (DSS) are two-phase alloys with approximately equal proportions of bcc ferrite (α) and fcc austenite phases (γ). The combination of properties of both phases, i.e., high strength and stress-corrosion resistance, has made DSS attractive for many purposes. Recently, a low-alloyed grade of DSS named Lean DSS (LDSS) has been introduced in the market. In this new family of economical duplex stainless steels, the expensive Ni is substituted by N or Mn. Lean duplex stainless steel can certainly improve the progress of the duplex stainless steels as it is possible to retain quality at reduced cost [1,2].

In general, fatigue damage consists of the following stages: (i) substructural changes causing cyclic strain localization, (ii) short crack initiation and (iii) growth and coalescence of initiated short cracks to form a dominant macro-crack that finally produces the failure of the material. Crack nucleation is usually controlled by the plastic deformation developed during fatigue. It is expected that at sites, where local cyclic plastic deformation is concentrated, cracks nucleate. The fatigue short crack nucleation and subsequent propagation in polycrystalline metals and alloys not only strongly depend on microstructure but also are influenced by the loading conditions, i.e., temperature, strain rates and stress amplitude. In DSS there are several microstructural factors that affect fatigue damage, such as orientation relationship between the phases, partitioning of alloying elements to different phases, texture, and topography [3–6]. Regarding the fatigue loading variables imposed on the test, it should be taken into account that different physical mechanisms are involved in LCF and HCF regimes being relevant for eventual fatigue failure. Whereas LCF leads to a relatively homogenous macro-plastic deformation within all grains and the dislocation slip is active in a large number of grains, in the HCF regime only a fraction of favorably oriented grains show plastic deformation. In this sense, the study of damage evolution in the aged duplex stainless steel (German designation DIN 1.4462) has revealed different microcrack behaviors during LCF and HCF [7]. During LCF, microcracks initiate within the ferrite phase or at the α/α grain boundaries following microbands that develop parallel to the most favorable slip planes with the highest SF. The cracks propagate along slip planes with the highest SF in the neighboring grain (either ferrite or austenite). In the HCF regime, fatigue damage is generally initiated within the softer austenite phase by slip band formation followed by crack initiation either at α/α or α/γ boundary where austenitic slip bands intersect. To date there has been little to no information available on microcracks behavior in LDSS [8,9]. Strubbia et al. [9] studied short crack initiation and growth during low (LCF) and high cycle fatigues (HCF) in AL 2003 (UNS S32003). There, it was reported that whereas in HCF cracks nucleate at grain boundaries, during LCF cracks nucleate along intrusions/extrusions in ferritic grains and as they reach austenitic grains grow along active slip systems or by double slip activation.

* Corresponding author.
E-mail address: strubbia@ifir-conicet.gov.ar (R. Strubbia).

http://dx.doi.org/10.1016/j.msea.2014.07.076
0921-5093/

The aim of this work is to study microstructural short crack nucleation and propagation during LCF as well as short cracks nucleation during HCF in LDSS LDX 2101. Moreover, the correlation of microcracks behavior with the dislocation structure developed in both fatigue regimes is attempted. These results are compared and analyzed with those previously reported for LDSS AL 2003 [9].

2. Material and experimental procedure

2.1. Material

The investigated material was the LDSS LDX 2101 (UNS S32101). This steel was received in a longitudinally welded stainless steel pipe. The manufacturing process of the pipes includes a hot rolled stage and a subsequent welding of the tube. A thermal treatment at 1050 °C followed by a rapid water quench was finally carried out to the tube. The chemical composition of the present LDSS in weight percentage is C:0.026; Cr:21.53; Ni:1.53; Mo:0.28; Mn:4.9; Si:0.63; P:0.021; N:0.22; and Fe: balance. The yield stress of the LDX 2101was measured as $R_{p0.2}=530$ MPa. From slabs taken parallel to the axis of the pipe and flat specimens for low and high cycle fatigue were machined. Fig. 1(a) shows the geometry of the specimen used for fatigue tests. An optical micrograph from the as-received LDSS is given in Fig. 1(b). The microstructure morphology consists mainly of a lamellar structure of bright austenite islands embedded in a grey etched ferrite matrix. The EBSD technique was used to determine grain size and volume fraction of the phases. The strength of both phases was estimated by Vickers hardness measurements. Table 1 shows the average grain size, standard deviation, standard error of the mean and volume fraction of each phase in LDX 2101 and in AL 2003. The microstructural features and chemical composition of this last grade are added for comparison purposes [9].

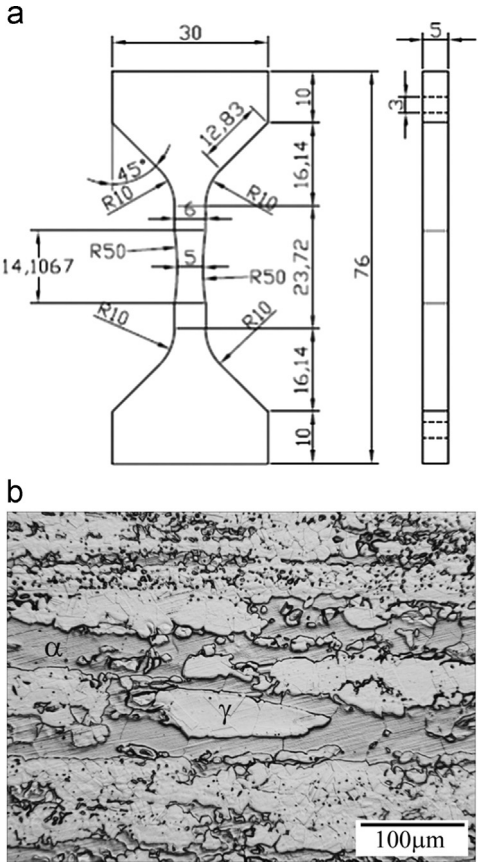

Fig. 1. (a) Specimen geometry and (b) microstructure of LDX 2101.

2.2. Specimen preparation

Specimens for mechanical tests were initially ground (down to 1200 grid SiC paper), polished (down to 3 μm diamond paste) and finally electrolytically polished, using Struers A2 electrolyte. This surface preparation allows the observation of the structure during tests and the acquisition of good quality electron back-scattered diffraction patterns (EBSD).

2.3. Mechanical tests

In order to observe the damage evolution during LCF tests, a central sector of the specimens was selected. Surface damage observations of this zone were performed by in situ microscopy before and during the LCF test using an optical system composed of a CCD camera JAI model CM-140MCL with a 50× objective, focal length of 13 mm, depth of field of ±1 μm and a 12× ultra zoom device (giving a magnification of 600) mounted on the fatigue test machine. LCF tests were conducted at room temperature under fully reversed plastic strain control, at a constant total strain rate of $\dot{\varepsilon}=2\times10^{-3}\,s^{-1}$, with a plastic strain range of $\Delta\varepsilon_p=0.2\%$. The LCF test with these conditions was repeated five times so as to discern the occurrence of the initial slip lines with the surface relief in each phase and to calculate their corresponding standard deviations.

Besides, push–pull HCF tests were carried out in a servo-hydraulic testing system at room temperature under stress control with stress amplitude of $\Delta\sigma/2=425$ MPa, a stress ratio of $R=-1$ and a frequency of $f=10$ Hz. In situ observation of specimens during HCF was not possible because the optical system mounted on the HCF testing machine does not allow the discerning of small grains of the LDX 2101. This optical system is composed of a long-distance QUESTAR optical microscope coupled with a digital camera.

In order to compare the strain rates in LCF and HCF tests, the total strain rate of HCF tests was estimated. This quantity was approximated as the ratio between twice the total strain range measured at midlife to fracture (Nf/2) and the frequency, resulting in that$\dot{\varepsilon}$is of the order of $1\times10^{-1}\,s^{-1}$.

2.4. Slip systems determination

After LCF and HCF tests, a scanning electron microscope (SEM) equipped with EBSD detector was used. EBSD measurements provide the Euler angles (φ_1, Φ, φ_2) that characterize the three-dimensional orientation of the grains. These data enable the determination of the slip systems, their SF and their angles relative to the tensile axis. On the other hand, the angles between the surface slip markings and the loading axis were measured. The comparison of these angles with the calculated ones permits identification of the activate slip systems and their corresponding SFs.

2.5. TEM observation

In order to analyze the dislocation structure after fatigue, thin foils were prepared from discs cut parallel to the tensile axis of the specimen using a double-jet electropolisher. The dislocation structures of the as-received material and of the specimens cycled up to failure were observed by TEM (Philips EM 300).

Table 1
Grain size, volume fraction of phases and Vickers hardness of each phase in both LDSSs.

Material	Phase	Average diameter (μm)	Standard deviation (μm)	Standard error of the mean (μm)	Volume fraction of phases	Vickers hardness (HV)
LDX2101	**Ferrite**	4	2	0.2	0.31	260 ± 10
	Austenite	5	3	0.3	0.69	330 ± 20
AL2003	**Ferrite**	7	4	0.6	0.48	310 ± 10
	Austenite	4	2	0.1	0.52	320 ± 20

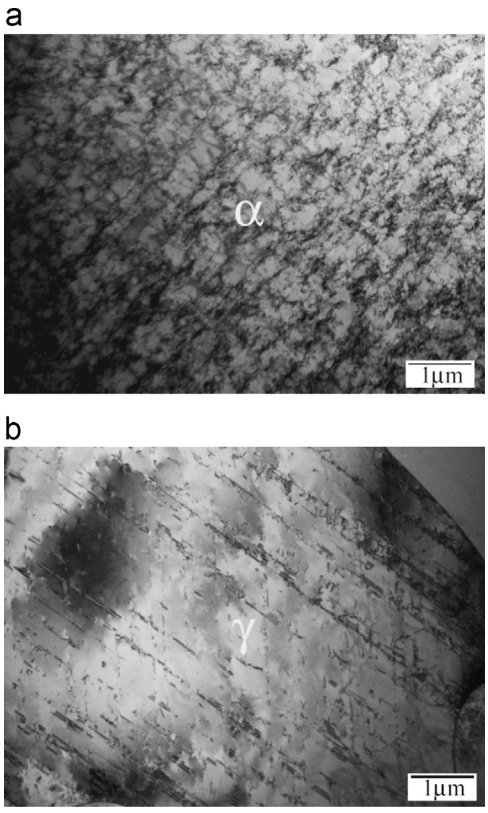

Fig. 2. Dislocation structure of LDX 2101 in the as-received condition (a) ferrite and (b) austenite.

3. Results and discussion

Fig. 2 shows the dislocation structure of both phases of LDX 2101 in the as-received condition. It is important to remark that after the thermomechanical manufacturing process, considerable dislocation density remains in both phases.

The in situ observation of LDX 2101 specimens subject to LCF tests reveals that the first slip markings appear almost simultaneously in both phases after 100 ± 50 cycles, Fig. 3(a). However, when cycling progresses the intensification of slip marking occurs mainly in the ferrite phase, Fig. 3(b). It is further noted that the development of surface damage takes place principally in the ferritic phase, increasing both quantity and intensity of slip markings, Fig. 3(c). Although the intensities of the slip markings in the austenitic phase increase during cycling, they are less than those observed in the ferritic phase. According to Lillbacka et al. [4], the elastoplastic properties and the distribution of the load between the phases in DSSs affect the amount of plastic strain supported by each phase during the fatigue test. These authors found that always the austenite has a higher hardening rate than the ferrite, when the austenite is the harder one of the two phases initially, the ferrite will bear almost all of the plastic deformations. Then, as in the LDX 2101, the austenite is harder than the ferrite

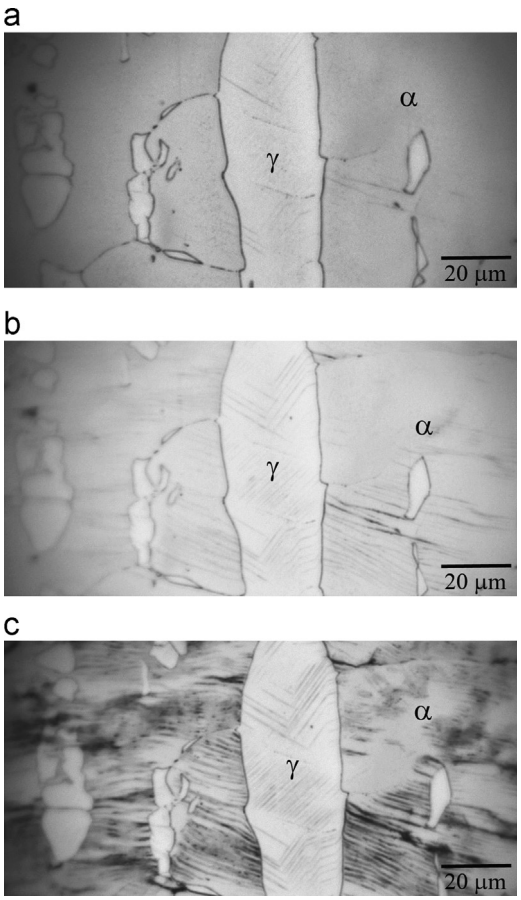

Fig. 3. Slip markings at the surface of LDX 2101 specimens subject to LCF after: (a) 100 cycles (b) 1,000 cycles and (c) 11,000 cycles.

(Table 1), it is expected that the ferrite experiences a higher plastic deformation than the austenite. Furthermore, it is well known that in DSS nitrogen addition not only causes an increase of the hardness of austenite but also promotes planar slip in this phase [10–13]. The planar nature of austenite restricts the sliding movement of dislocations to its slip plane. Hence, it is easier for the ferritic phase to accommodate the strain.

Strubbia et al. [9] recently observed in LDSS LDX 2101 and in AL 2003 that some of the slip lines in ferrite evolve to extrusions at the surface, where short cracks finally nucleate. The sites of fatigue short crack in LDSS LDX 2101 were corroborated in this work. Moreover, when a crack, originally nucleated within a single slip band in the ferritic phase, overcomes the phase boundary it resumes growing in a transgranular mode. Within this last phase, the crack path follows by sections of slip planes with high SF (stage I), Fig. 4(a). In other cases, the applied stress is not high enough to activate a source of dislocations in the neighboring grains, hence the crack is not able to surpass the microstructural barrier, and grows along phase boundaries, Fig. 4(b). Furthermore,

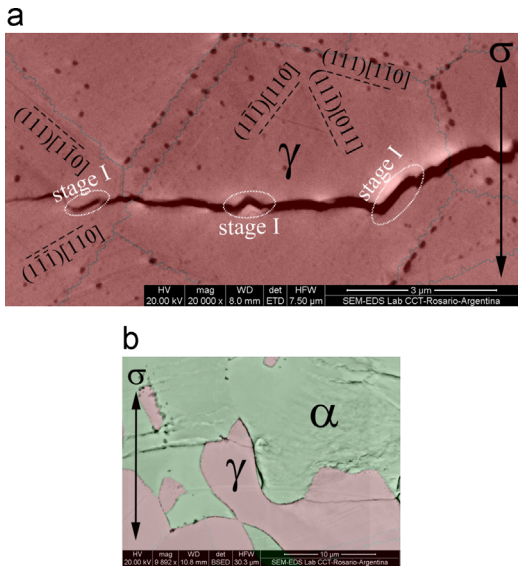

Fig. 4. Growth of LCF short cracks in LDX 2101 along (a) sections of slip planes with high SF and (b) phase boundaries.

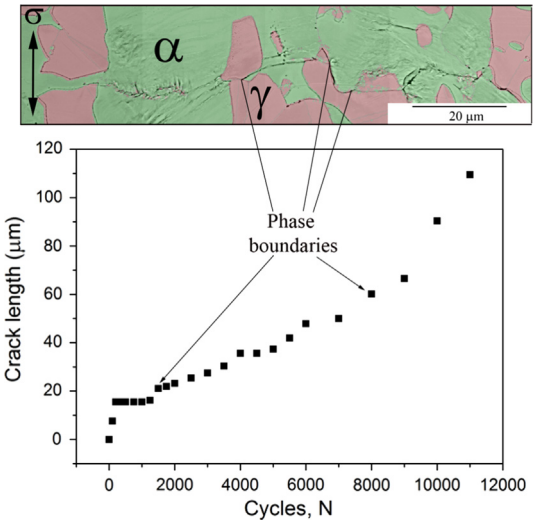

Fig. 5. Superposition of SEM image and EBSD phase map showing the crack path after LCF test and the crack length vs. number of cycles.

in LDX 2101 the crack growth direction is approximately perpendicular to the specimen axis.

For LDX 2101 subjected to LCF, crack lengths were measured and plotted with respect to the number of cycles, Fig. 5. These measurements allowed the estimation of a crack propagation law. It can be seen in this figure that in the present steel, as already reported in AL 2003 [9] and in standard DSSs [14,15], the microcrack growth follows an exponential law (cf. Paris law for long fatigue cracks). Additionally, Fig. 5 shows the phase distribution, obtained by the EBSD technique, overlapping the SEM image of the crack. From the correlation of this image with the crack growth behavior, it is worth mentioning that the growth rate of the cracks is strongly affected when the barrier to surpass is a phase boundary but not when it is just a grain boundary. Tokaji et al. [16] studied the growth of small fatigue cracks in a wide range of metals including a low carbon steel (S10C), a medium carbon steel (S45C), a high tensile steel (HT60), a low alloy steel (SCM435), a dual-phase stainless steel (SUS329J1), an aluminum alloy (7075-T6) and pure titanium (TB35C) and concluded that the short crack behavior is quite similar for those materials. In fact, the speed of short cracks growth decreases substantially when approaching a grain boundary, triple point or interphase.

In order to correlate the surface damage with the dislocation structure of fatigued specimens, thin foils were prepared from specimens cycled up to failure (16,000 cycles). In LDX 2101 the substructure in the austenitic grains is characterized by planar slip with at least two activated slip systems, Fig. 6(a). Also, stacking faults can be observed in most austenitic grains. However, the ferritic phase develops a higher plastic activity than the austenitic phase. Within the ferritic grains mixed substructures are found, including loop patches, walls and ill-formed cells, see Fig. 6(b) and (c). Moreover, some ferritic grains form a dislocation arrangement that resembles the characteristic ladder-like structure typical of persistent slip bands (PSB), Fig. 6(d). Such dislocation structure is a typical example of localization of the plastic strain which gives rise to microcrack nucleation [17,18]. Therefore, during LCF the crack nucleation in ferritic phase can be rationalized by a higher plastic activity in this phase with respect to that present in austenitic grains and by the strain localization in the α phase. The short crack propagation rate not only depends on the properties of boundaries but also on the degree of plasticity developed in the adjacent grain [5]. In this respect, Fig. 5 gives evidence that microstructural barriers, particularly the phase boundaries, deccelerate the growth rate of microcracks. In fact, the development of higher plastic activity in ferritic grains results in a dislocation microstructure which promotes crack advance. Therefore, it is easier for the crack to surpass a grain boundary α–α than a phase boundary α–γ. On the other hand, a reduction of growth rate was not observed when a crack reaches a γ/γ boundary and this fact was attributed to test design. The tests for the in situ observations were stopped to prefixed number of cycles so probably cracks were anchored in a microstructural barrier by a number of cycles less than the spacing between observations. Hence the perturbation of the growth rate goes unnoticed.

During HCF, the in situ observation of specimens was not possible, so in this case the surface damage in fractured specimens was analyzed. SEM and EBSD measurements reveal that while in AL 2003 most of the cracks nucleate at grain boundaries [9], in the LDX 2101 cracks nucleate along intrusions/extrusions in the ferritic phase, Fig. 7.

TEM observations of LDX 2101 subjected to HCF show that the ferrite phase presents grains with different dislocation structures such as cells (Fig. 8(a)) and dislocation microbands (Fig. 8(b)). Conversely, the austenitic phase exhibits a microstructure similar to that observed in the as-received condition, Fig. 8(c). It can be concluded from these results that the ferritic phase supports most of the plastic deformation. This strain partition is mainly due to the higher hardness of austenite with respect to the ferritic phase. Therefore, the cracks nucleation in intrusion/extrusion within the ferritic phase of LDX 2101 could be attributed, just as in LCF, to its higher plastic activity and strain localization mainly in microbands. In contrast, it was found [9] that in AL 2003 subjected to HCF the ferrite phase exhibits a microstructure similar to that observed in the as-received condition whereas the austenite phase presents pile-ups of dislocations on one, two or three active slip systems. These pile-ups are arrested at grain boundaries generating zones of high localized stresses and consequently a high dislocation density, where finally short cracks nucleate.

The dislocation structure and crack nucleation sites depend on the plastic deformation sustained by each constituent phase. Mughrabi [19] shows that the mechanical behavior of the ferrite phase depends strongly on temperature and strain rates, $\dot{\varepsilon}$. This fact is rationalized by the extended core structure of screw dislocations which makes them sessile at low temperatures or higher strain rates. Its transformation to mobile dislocations can be assisted by thermal activation or stress which contribute to

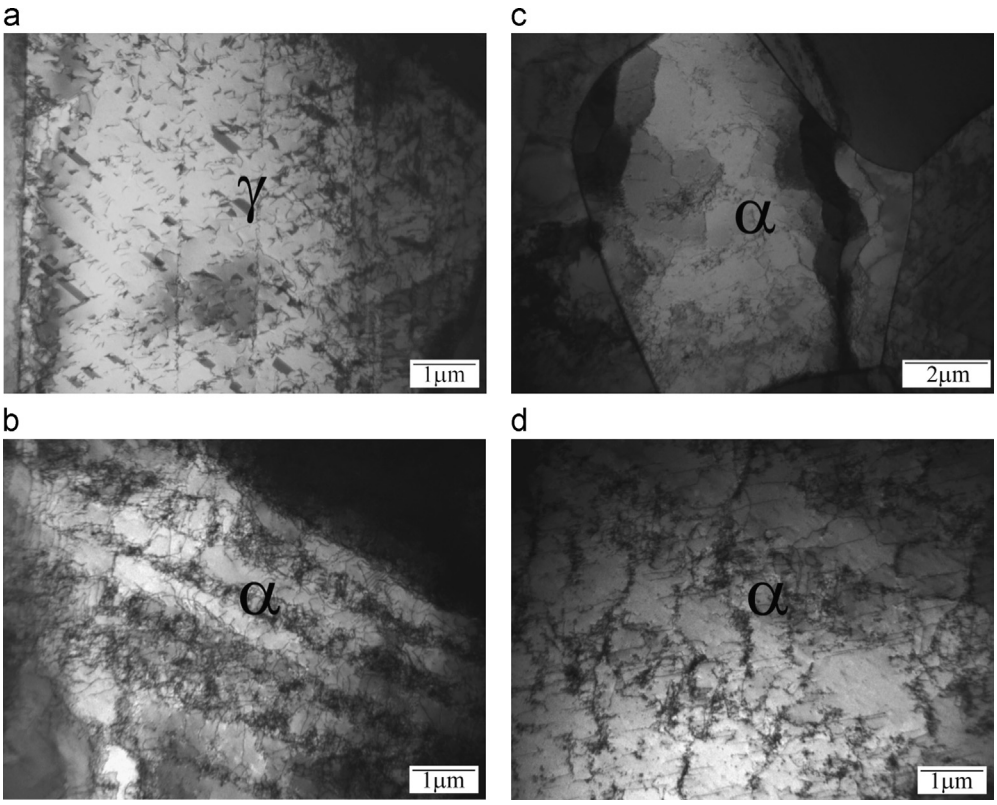

Fig. 6. Dislocation structure in LDX 2101 specimens subject to LCF up to failure (a) austenite and (b), (c) and (d) ferrite.

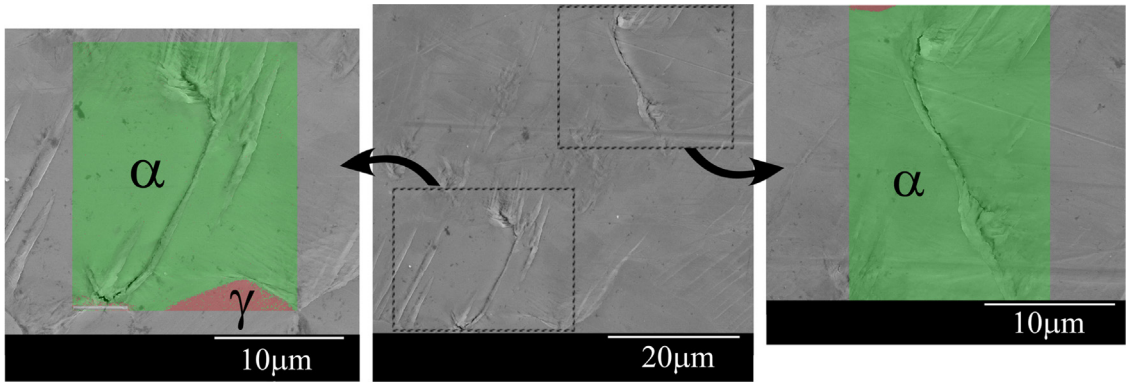

Fig. 7. SEM image and EBSD map showing cracks nucleation along intrusions/extrusions in ferritic phase in HCF specimens.

surpass the lattice friction stress (Peierls–Nabarro stress) associated with the extended core [20]. Therefore, at temperatures below a transition temperature T_0 (T_0 is between 0.1 and 0.2 T_m, T_m: melting temperature) the mobility of screw dislocations strongly decreases. This temperature is shifted to markedly higher temperature at higher strain rates. It is assumed that at moderates strain rates ($\dot{\varepsilon} \leq 10^{-4}\ s^{-1}$) the transition temperature lies around room temperature for the α-Fe (ferrite) [19].

Taking into account the high strain rate ($\dot{\varepsilon} \approx 1 \times 10^{-1}\ s^{-1}$) employed in HCF, room temperature can be considered well below T_0 and thus, screw dislocations will have limited mobility in the ferrite phase. Strubbia et al. [9] assume that due to this phenomenon, the restricted movement of screw dislocations in the ferrite phase of AL 2003 leads the austenite phase to sustain most of the plastic deformation. Moreover, these authors observed that as the pile-ups in the austenite impinge γ–γ , γ–α boundaries produce a zone of high stress concentration where microcracks nucleate. Crack nucleation at α–α boundaries could be attributed to asymmetrical slip of screw dislocations in the ferrite phase of LDSS AL 2003.

Though HCF tests in LDX 2101 were carried out at the same strain rate ($\dot{\varepsilon} \approx 1 \times 10^{-1}\ s^{-1}$) as in HCF in AL 2003, TEM observations suggest that in the ferrite phase of LDX 2101 the motion of dislocations is not hindered, Fig. 8(a) and (b). As already mentioned, if the effective stress is high enough sessile screw dislocations can become mobile. The harder ferrite in AL 2003 as compared to LDX 2101 prevents screw dislocation motion for the same test conditions. Thus, the higher dislocation density that can develop in the ferrite phase of LDX 2101 leads to plastic strain concentration in the form of microbands which enhances microcrack initiation.

In both fatigue regimens, LCF and HCF, the analysis of activated slip systems reveals that in the austenite grains most of the observed traces correspond to slip systems with SF higher than 0.4. This is consistent with the results reported in AL 2003 [9] and in 316L austenitic stainless steel [21]. The determination of the

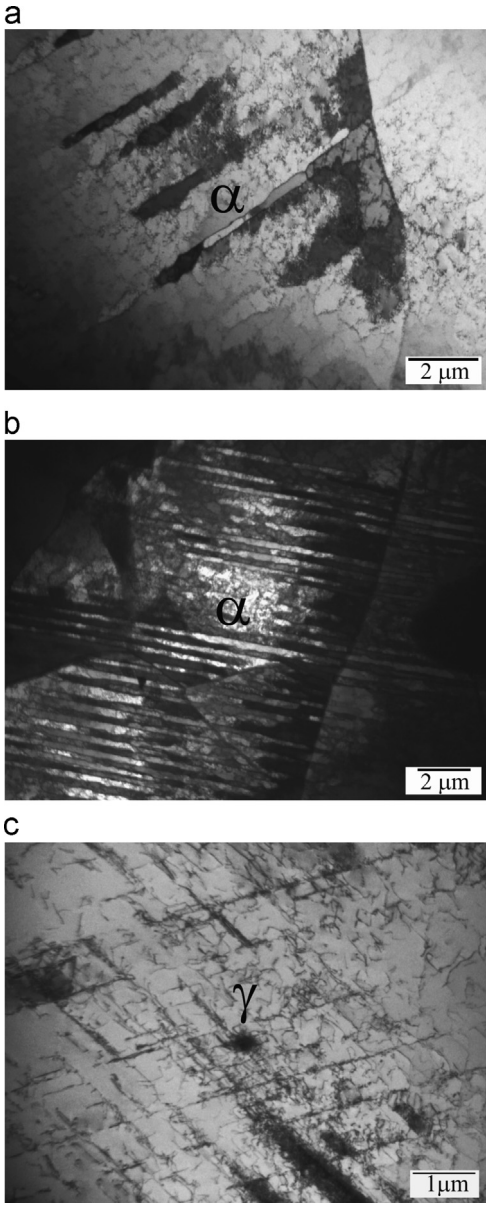

Fig. 8. Dislocation structure in LDX 2101 specimens subject to HCF up to failure (a) and (b) ferrite and (c) austenite.

active slip systems in the ferrite is very difficult. Nonetheless, through a detailed analysis it is found that in the ferritic grains some activated slip systems present SF below 0.4. This fact agrees with the results reported in LDSS AL 2003 [9], DSS [3,22,23] and in aged DSS [24]. Gironès et al. [24] reported that in the ferritic grains not only the SF define the development of plastic activity, but other parameters such as slip activity in the neighboring grains must also be considered, conversely, in austenitic grains the SF is the decisive parameter which defines the activation of their slip systems.

4. Conclusions

Substructural and fatigue damage features of LDSS LDX 2101 are analyzed leading to the following conclusions.

In both fatigue regimes, LCF and HCF, the active slip systems in austenitic grains have Schmid factors higher than 0.4. Conversely, some active slip systems observed in ferrite have SF lower than 0.4.

The plastic deformation is mainly sustained by the ferrite phase during LCF and HCF, a fact attributed principally to its lower harness in comparison to the austenite phase (for this particular material). This could explain the cracks nucleation along intrusions/extrusions in this phase.

During LCF, when cracks reach the ferrite–austenite phase boundary, they may overcome the boundary and resume growing in the neighboring austenitic grain, but in other cases the cracks may not able to surpass the microstructural barrier and grow along phase boundaries. Moreover, the growth rate of cracks is strongly affected by phase boundaries.

Acknowledgment

This work was supported by Agencia Nacional de Promoción Científica y Tecnológica, and Consejo Nacional de Investigaciones Científicas y Técnicas(CONICET) and by the Cooperation Program DAAD/MinCyT between Germany and Argentina.

The authors would like to thank Mr. Alexander Giertler for performing the HCF tests.

References

[1] J. Da-Wei, G. Chang-Sheng, Z. Xiang-Juan, L. Junl, S. Lu-Lu, X. Xue-Shan, J. Iron Steel Res. Int. 19 (2) (2012) 50–56.
[2] E. Alfonsson, Lean Duplex – the First Decade of Service Experience, in: 8th Duplex Stainless Steels Conference, Beaune, France, 2010.
[3] M-C Marinelli, A. El Bartali, J.W. Signorelli, P. Evrard, V. Aubin, I. Alvarez-Armas, S Degallaix-Moreuil, Mater. Sci. Eng. A 509 (2009) 81–88.
[4] R. Lillbacka, G. Chai, M. Ekh, P. Liu, E. Johnson, K. Runesson, Cyclic Stress–Strain Behavior and Load Sharing in Duplex Stainless Steels: Aspects of Modeling and Experiments, Acta Mater. 55 (16) (2007) 5359–5368.
[5] J. Stolarz, J. Foct, Mater. Sci. Eng. A 319–321 (2001) 501–505.
[6] A. Mateo, L. Llanes, N. Akdut, M. Anglada, Mater. Sci. Eng. A 319–321 (2001) 516–520.
[7] I. Alvarez-Armas, U. Krupp, M. Balbi, S. Hereñú, M.C. Marinelli, H. Knobbe, Int. J. Fatigue 41 (2012) 95–100.
[8] R. Strubbia, S. Hereñú, M.C. Marinelli, I. Alvarez-Armas, Int. J. Fatigue 41 (2012) 90–94.
[9] R. Strubbia, S. Hereñú, A. Giertler, I. Alvarez-Armas, U. Krupp, Int. J. Fatigue 65 (2014) 58–63.
[10] N. Akdut, J. Keichel, J Foct, Steel Res 68 (11) (1997) 495–500.
[11] G. Wahlberg, U. Rolander, H.O. Andren, in: J. Foct, A. Hendry (Eds.), HNS '88, Proceedings of the 1st International Conference on High Nitrogen Steels.
[12] Y. Li, C. Laird, Mater. Sci. Eng. A 186 (1994) 65–86.
[13] J. Foct, N. Akdut, Scr. Metall. Mater. 29 (1993) 153–158.
[14] J. Polak, P. Zezulka, Fatigue Fract. Eng. Mater. Struct. 28 (10) (2005) 923–935.
[15] M. Balbi, M. Avalos, A. El Bartali, I. Alvarez-Armas, Int. J. Fatigue 31 (11–12) (2009) 2006–2013.
[16] Z. Tokaji, T. Ogawa, in: K.J. Miller, E.R. de los Rios (Eds.), Short Fatigue Cracks, 13 ESIS, Mechanical Engineering Publications, London, 1992, p. 85–99.
[17] M.D. Sangid, Int. J. Fatigue 57 (2013) 58–72.
[18] J. Man, M. Petrenec, K. Obrtlík, Acta Mater. 52 (2004) 5551–5561.
[19] H. Mughrabi, Dislocations and Properties of Real Materials, vol. 323, 1985, pp. 244–261.
[20] J.C. Grosskreutz, M. Mughrabi, Chapter 7 Description of cyclic deformation, in: A.S. Argon (Ed.), Constituve Equations in Plasticity, MIT Press, Cambridge, 1975, pp. 251–317.
[21] P. Villechaise, L. Sabatier, J.C. Girard, Mater. Sci. Eng. A 323 (1–2) (2002) 377–385.
[22] J.B. Vogt, D. Salazar, and I. ProriolSerre, Chapter 8 Partition of cyclic plasticity in the 25Cr–7Ni–0.25N duplex stainless steel investigated by atomic force mycroscopy, in: I. Alvarez-Armas, S. Degallaix-Moreuil, Duplex Stainless Steels, 2009, pp. 275–302.
[23] A. El Bartali, V. Aubin, L. Sabatier, P. Villechaise, S. Degallaixmoreuil, Scr. Mater. 59 (12) (2008) 1231–1234.
[24] A. Gironès, P. Villechaise, A. Mateo, M. Anglada, J. Méndez, Mater. Sci. Eng. A 387–389 (2004) 516–521.